Current Science
CS 6 (1), 5846-5852 (2026)
Received 07 January 2026 | **Accepted 12 February** 2026 | **Online Available 15 February** 2026
https://doi.org/10.52845/CS/2026-6-1-15

Current Science

Current Science

OPEN ACCESS

ISSN(O) 2795-8639

Original Article

Rhodamine B Dye Photocatalytic Degradation Using Cu-Doped Zno Nanoparticles

Milind S. Deshpande[1], Digvijay. V. Sonawane[1], Shailesh S. Deshmukh[1], Anil E. Athare[2*]

[1]Post-Graduate Department of Chemistry, Pemraj Sarda College, Ahilyanagar, (Ahmednagar), (MS), India

[2]Vice-Principal, Post-Graduate Department of Chemistry, New, Art's Commerce and Science College, Ahilyanagar, (MS), India 414001

***Corresponding Author: Anil E. Athare**

Abstract:
Effective degrading techniques are required for environmental protection since rhodamine B (RhB) is a dye that poses a high risk of environmental pollution. ZnO is widely used in dye degradation because of its superior ultraviolet (UV) photocatalytic capability. Photocatalytic degradation technology provides a workable way to reduce such pollution. Cu-doped ZnO nanoparticles were effectively created in this work using a simple precipitation technique. The material demonstrated exceptional photocatalytic activity under UV irradiation when the Cu doping level was 0.8%; total RhB degradation was achieved in 5 hours (degradation efficiency up to 100%). The material's physical and chemical characteristics were methodically examined using transmission electron microscopy (TEM), scanning electron microscopy (SEM), and X-ray diffraction (XRD).The findings showed that while Cu insertion greatly improved ZnO's light response capabilities, it had no effect on the material's crystallinity. The photocatalytic mechanism of Cudoped ZnO was fully explored based on the experimental results of UV-catalyzed RhB solution degradation, offering theoretical insights and technological assistance for the creation of high-efficiency photocatalysts for dye degradation.

Keywords: Rhodamine B, Cu-doped ZnO, UV light exposure.

1. Introduction

Due to the large volume of industrial waste that is dumped into natural bodies of water, water pollution is a serious ecological problem that is expected to worsen in the future. The Fenton process and photocatalysis are two popular techniques for eliminating pollutants that are both quite practical [1]. By photodegrading contaminants (organic or inorganic) into simpler and non-toxic components, photocatalytic materials offer a viable and well-researched method of treating wastewater. The majority of dyes are composed of substances with robust chemical and physical characteristics that are highly soluble and stable in water [2]. Long-term buildup in the natural world can result in harmful effects and reduced light penetration in water, among other threats to human health and the ecosystem. Nevertheless, dye contamination of water remains a significant issue that has not been resolved. Rhodamine B, one of the many synthetic textile dyes, has the potential to be carcinogenic, mutagenic, and cardiotoxic. Rhodamine B exposure or consumption can result in respiratory difficulty, gastrointestinal trouble, skin irritation, eye irritation, and even death. The

anaerobic digesting process is one of the conventional degradation techniques for water contaminants [3, 4]. However, because of their intrinsic benefits, photocatalytic technologies have become more popular, and their modification techniques have also interacted with other chemical and physical processes. For example, adding substances like peroximonosulfate, persulfate, or $NaBH_4$ (sodium borohydride) can stimulate (catalyze) photocatalytic processes, which could improve the degradation efficiency. Additionally, photocatalytic technology has been used in processes including ammonia synthesis and hydrogen production. For the breakdown of organic pollutants, the photocatalytic method utilizing semiconductor nanoparticles such TiO2, ZnO, Fe_2O_3, and ZnS is thought to be an efficient technology. The most widely available and often utilized semiconductor materials among them are ZnO and TiO2.ZnO has a high efficiency as a photocatalyst due to its significant absorption of ultraviolet light in the solar spectrum, making it an effective oxidant. ZnO is more effective than other catalysts at producing H2O2, which is useful for breaking down colors in water. A photocatalytic process, in which electrons from the valence band are stimulated to the conduction band, takes place when ZnO materials are exposed to UV light in water [5, 6]. This mechanism creates holes (h+) in the valence band and electrons in the conduction band. Superoxide anion radicals (O_2*) are created when electrons react with oxygen molecules in water, and hydroxyl radical compounds (OH*) are created when holes react with hydroxyl ions in water [7]. The molecule H_2O_2 is created when the superoxide radicals continue to react with the electrons and the H+ ions in the water. The hydroxyl radical is created when this H_2O_2 molecule interacts with the electrons once more. In actuality, ZnO's performance is inadequate for industrial uses. Therefore, it is necessary to improve ZnO's optical characteristics so that it can generate electrons using UV light energy [8]. Doping transition metals is one technique for enhancing ZnO performance that has attracted a lot of interest. This modification method creates new energy levels in the band gap by introducing flaws into the main lattice. Therefore, it is fair to anticipate that the addition of transition metal ions to ZnO will support possible modifications in their physical and optical properties, given the significance of metal ions in optical applications.

ZnO has been synthesized using a variety of techniques [9, 10]. Due to its advantages of low cost, high toxicity, and ecological friendliness, environmentally friendly ZnO synthesis is a prominent method among chemical synthesis techniques. In this work, Zn (OAC) •2H2O was used as the raw material to create Cu-doped ZnO composites utilizing a straightforward solvothermal method [11]. Because of the lower rate of electron–hole pair recombination, the Cu-doped ZnO composites demonstrated exceptional photocatalytic activity. This report differs from others. Furthermore, Rhodamine B (RhB) dye degradation in aqueous solutions was assessed using the produced catalyst's photocatalytic performance [12]. Energy dispersive X-ray spectroscopy (EDX), scanning electron microscopy (SEM), X-ray diffraction (XRD), specific surface area and porosity analysis (BET and BJH), and transmission electron microscopy (TEM) were among the methods used to characterize the structure and characteristics of the photocatalysts [13] . Lastly, a theory explaining how Cu doping affects ZnO's photocatalytic activity is put forth. Additionally, the synergistic effect of Cudoped ZnO on RhB degradation is examined [14, 15].

2 Materials and Methods

Preparing the catalyst creation of nanoscale zinc oxide samples through calcination at a high temperature. Copper Ammonium bicarbonate ($CuH_6N_2O_9$) and zinc (II) acetate dihydrate ($C_4H_{10}O_6Zn$) were dissolved in 100 ml of

deionized water. The intermediate sediment is gathered and cleaned three times with ethanol and water after it has stood for a while. The precipitates were maintained warm for three hours in a drying box with a constant temperature of 120 °C. In order to create nano-ZnO (ZnO NPs), the aforementioned materials were finally pulverized, moved to a muffle furnace, and calcined at 500°C for three hours. A certain amount of ZnO NPs was mixed with 1%, 2%, 3%, 4% and 5% ammonium bicarbonate (w %), dissolved in ethanol, and agitated in a water bath at a constant temperature of 80°C until the ethanol entirely evaporated. Copper-doped ZnO nanocrystalline was generated by calcination in a muffle furnace at 500°C for three hours following solid grinding.

Results and Discussion

XRD Analysis

We used X-ray diffraction analysis to independently confirm the crystal structure of our samples; the matching XRD patterns are displayed in Figure 1. According to the data, there are numerous distinctive sharp peaks that correlate to the ZnO crystal planes (100), (002), (101), (102), (110), and (103) [16, 17]. The wurtzite hexagonal phase of ZnO can be identified from the associated peaks and all diffraction patterns. Moreover, no additional impurity peaks are found following Cu-doping, indicating that Cu-doping has not caused structural alterations in ZnO. The findings demonstrate that the microstructure of ZnO is unaffected by Cu doping [18]. Additionally, the catalyst samples' crystal type remained unchanged both before and after doping, suggesting that they were stable. BET analysis was performed on NPs and ZnO without Cu doping to examine the impact of Cu doping on the surface structure of ZnO [19]. ZnO catalysts and 1% Cu/ZnO NPs' Na adsorption–desorption curves clearly show the H_4 hysteresis ring [20, 21]. Both ZnO without Cu and 0.1% Cu/ZnO NPs catalysts exhibit macro porous or meso porous surface architectures, as seen in Figure 1, where the adsorption increases quickly in the high pressure area (p/p0=0.8–1.0) [22, 23]. The catalyst's specific surface area and pore size have an impact on its catalytic performance. The material's photo catalytic performance can be significantly enhanced by the large specific surface area and narrow pore structure, which can offer additional active sites for the photo catalytic process [24]. There are additional opportunities to enhance the catalyst's adsorption and catalytic activity when the specific surface area increases. The specific surface area of Cu ions is greatly increased after doping, which aids in exposing more active sites [25], shown in Figure 2.

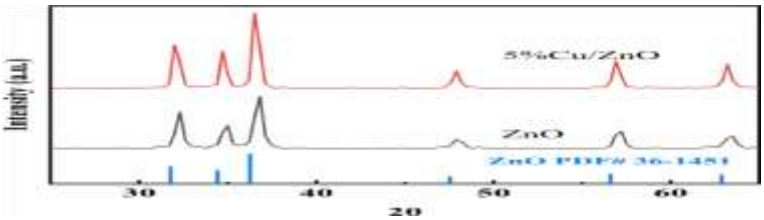

Figure 1: The XRD patterns of ZnO

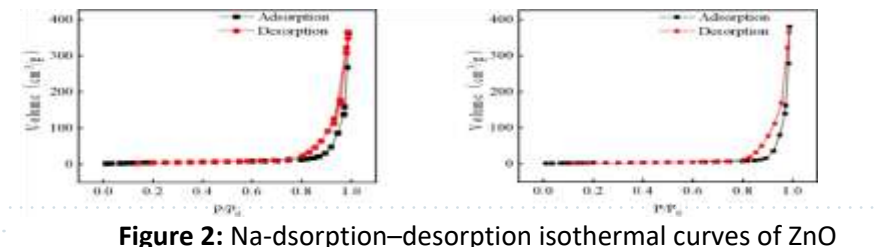

Figure 2: Na-dsorption–desorption isothermal curves of ZnO

SEM Analysis

Scanning electron microscopy (SEM) pictures of pure ZnO are shown in Figure 3, whereas SEM images of ZnO samples doped with 1 % copper and generated under the same calcination conditions are shown. According to the SEM study, the undoped ZnO particles are about 55 nm in size, and some of them have very noticeable clustering behaviour [26]. The copper-doped ZnO samples on the other hand, show lower particle sizes and less clumping, with the particles taking on a distinctive hexagonal structure. The introduction of copper ions into the ZnO crystal lattice, which decreases the system's energy state, is thought to be the cause of this morphological change [27]. Furthermore, diffusion-induced segregation along grain boundaries may be driven by the concentration gradient of copper ions between the inside and outside of the crystal grains, preventing additional crystal development. The results of pertinent studies are consistent because there was no discernible change prior to or following the reaction due to the catalyst's uneven shape [28].

TEM and EDX Analysis

The microstructure of ZnO is visible from the TEM image in Figure 4. The lattice stripe width of the ZnO high-exposure crystal plane is represented by d=0.45. The samples were also subjected to EDS testing in order to examine their elemental distribution. The results Figure 4 show that the elements copper (Cu), zinc (Zn), and oxygen (O) are dispersed over the whole sample region. This further demonstrates that Cu/ZnO photocatalysts were successfully produced. The 1% Cu/ZnO catalyst's fluorescence spectra were obtained at a wavelength of 370 nm using single-photon excitation [29]. A clear peak is seen about 470 nm, as shown in Figure 5. According to a survey of the literature, pure ZnO usually has fluorescence peaks between 430 and 470 nm. Zinc vacancies are responsible for the peak at about 430 nm, as shown in Figure 4. Only the 475 nm peak, which is the green emission peak brought on by radioactive recombination, is seen in the present investigation [30]. Deep-level defect radiations, specifically the recombination of photo generated holes and singly ionized electrons on oxygen vacancies during photo catalysis, are the source of this green emission peak.

UV Analysis

A layer of Cu^{+} will cover the surface of nano ZnO as the Cu-doped level gradually rises [31]. ZnO absorbs less light when exposed to UV light, which naturally reduces its catalytic activity. ZnO shows good UV deterioration, according to Figure 5.

Photocatalytic activity

Copper doping may be the cause of the lack of the 435 nm peak, which is suggestive of zinc vacancies, but this does not prevent photo generated holes and singly ionized electrons localized on oxygen vacancies from recombining during the photo catalytic process. The enhanced defect density brought on by copper doping may be the reason why the defect peak in the Cu-doped materials exhibits notable intensity, similar to that of excitonic emission. The deterioration rate curves of various Cu-doped ZnO samples following calcination at 400°C for six hours using Rhodamine B solution are displayed in Figure 6. According to experimental data on Rhodamine B degradation by photocatalysts, nearly total degradation of Rhodamine B is accomplished at a copper doping level of 1% after 125 minutes of UV irradiation [32, 33]. As the copper doping level is increased, the solution's final deterioration rate fluctuates and gradually decreases. According to the investigation, this could be because copper ions absorb electrons produced during the photocatalytic process. As a result, the likelihood of collisions between electrons and holes produced during the photocatalytic process

diminishes over time, and the solution's deterioration is accelerated by the growing number of remaining holes.

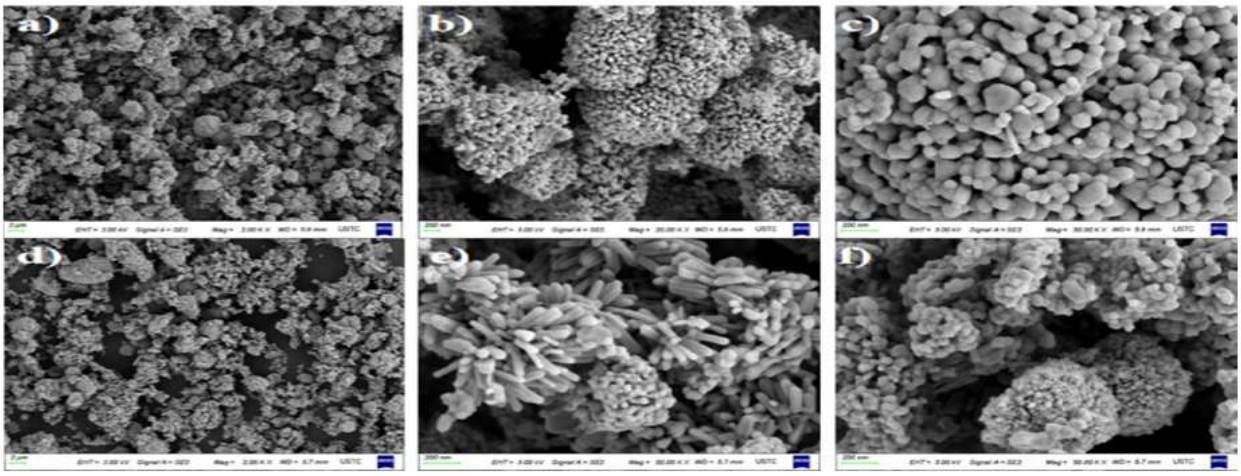

Figure 3: SEM image of Cu doped ZnO, Nps

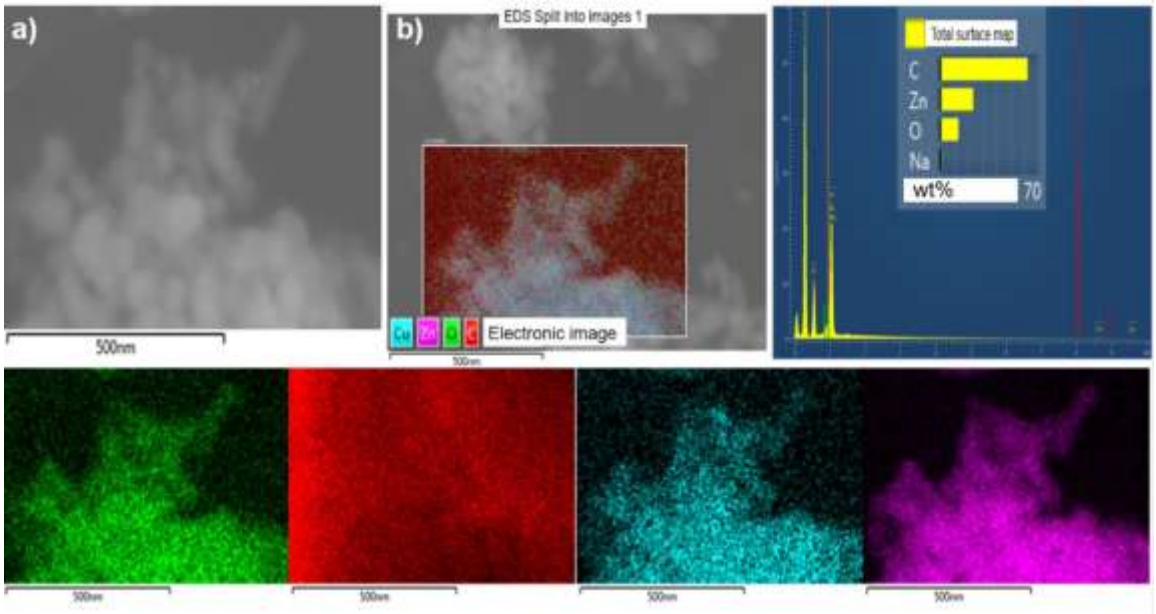

Figure 4: Energy spectrum analysis of 0.5% Cu/ZnO

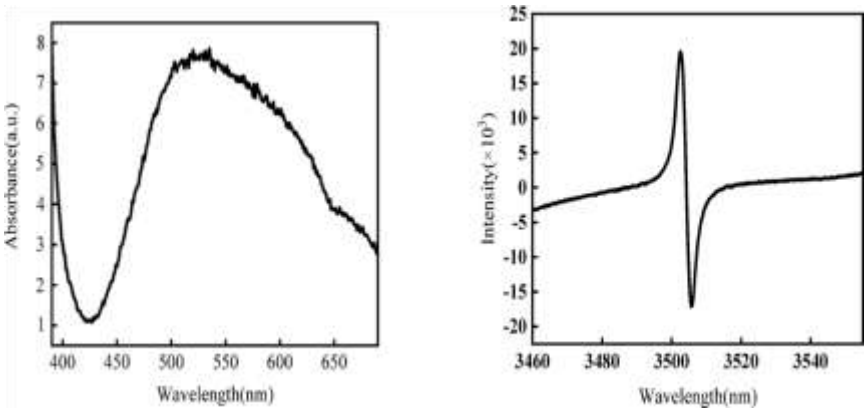

Figure 5: UV absorption spectrum

The degrading effectiveness of ZnO towards Rhodamine B solution is greatly increased by mild Cu doping. The maximum photocatalytic activity is shown by the composite photocatalyst material, 1% Cu/ZnO. By absorbing photon energy, ZnO's valence band is excited. This results in excitonic electrons (e−), which move to ZnO's conduction band and leave behind a hole in the valence band. The photocatalytic activity is facilitated by the resultant band gap energy. Figure 6, illustrates the photocatalytic degradation of Cu-doped ZnO. According to pertinent data, research has been done on how various pH levels affect degradation. Reactions are carried out in our lab at a gentle pH. Following their transfer to the ZnO crystal's surface or the Cu^{2+} surface via the ZnO, the excitonic electrons and holes can react with O_2 and H_2O or OH^- in the solution to create photocatalytically active $\bullet O^{2-}$ and •OH free radicals. The following are the reaction equations [34, 35].

$$O2 + e - \rightarrow \cdot O^{-2} \quad (1)$$

$$H_2O + H^+ \rightarrow \cdot OH + H^+ \quad (2)$$

$$OH^- + H^+ \rightarrow \cdot OH \quad (3)$$

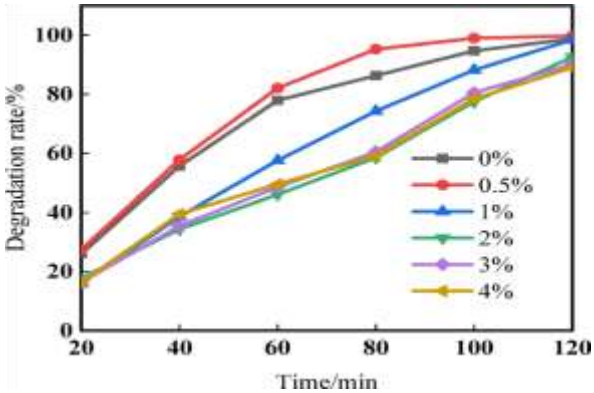

Figure 6: Photocatalytic degradation efficiency of Rhodamine B.

Conclusion

The synthesized ZnO provide high yield of Cu doped ZnO nanoparticles. The obtained ZnO have high photocatalytic activity in decomposing dyes. The current work can be applied to synthesize other Cu doped metal oxides that can be applied as catalysts in degrading and treatment of industrial water from harmful dyes.

Acknowledgements

Authors are thank the Department of Physics Savitribai Phule Pune University, Pune, for providing Characterization of nanomaterials.

References

1 Benhelal, E.; Zahedi, G.; Shamsaei, E.; Bahadori, A.; *J Cleaner P*rod, **2013,** 51, 142.

2 **Machado, S.; Pacheco, J. G.; Nouws, H. P. A.; Albergaria, J. T.; Delerue-Matos, C.** *Sci. Total Environ.*, **2015**, **533**, 76–81.

3 **Das, S.; Srivastava, V. C.** *Smart Sci.*, **2016**, **4**, 190–195.

4 **Hasan, S.** *Res. J. Recent Sci.*, **2015**, **4**, 1–3.

5 **Khan, I.; Saeed, K.; Khan, I.** *Arab. J. Chem.*, **2019**, **12**, 908–931.

6 **Kharat, S. N.; Mendhulkar, V. D.** *Mater. Sci. Eng. C*, **2016**, **62**, 719–724.

7 **Kumar, S. S.; Venkateswarlu, P. R.; Rao, G. N.** *Int. Nano Lett.*, **2013**, **3**, 1–6.

8 **Jana, N. R.; Earhart, C.; Ying, J. Y.** *Chem. Mater.*, **2007**, **19**, 5074–5082.

9 **Jiang, H. L.; Xu, Q.** *Catal. Today*, **2011**, **170**, 56–63.

10 **Yadav, T. P.; Yadav, R. M.; Singh, D. P.** *Nanosci. Nanotechnol.* **2012**, **2**, 22–48.

11 **Yang, W.; Wang, L.; Mettenbrink, E. M.; Deangelis, P. L.; Wilhelm, S.** *Annu. Rev. Pharmacol. Toxicol.*, **2021**, **61**, 269–289.
12 **Triana, M. A.; Hsiang, E. L.; Zhang, C.; Dong, Y.; Wu, S. T.** *ACS Energy Lett.*, **2022**, **7**, 1001–1020.
13 **Nazari, A.; Riahi, S.** *Compos. Part B*, **2011**, **42**, 570–578.
14 **Osuntokun, J.; Ajibade, P. A.** *Phys. B Condens. Matter*, **2016**, **496**, 106–112.
15 **Huang, X.; Boey, F.; Zhang, H.** *Chem. Soc. Rev.*, **2012**, **41**, 666–686.
16 **Machado, S.; Pacheco, J. G.; Nouws, H. P. A.; Albergaria, J. T.** *Sci. Total Environ.*, **2015**, **533**, 76–81.
17 **Laad, M.; Jatti, V. K. S.** *J. King Saud Univ. Eng. Sci.*, **2016**, **28**, 1–6.
18 **Teng, W.; Jeng, S.; Kuo, C.; Lin, Y.; Liao, C.; Chin, W.** *LiQ. Cryst.*, **2008**, **33**, 1663–1665.
19 **Machado, S.; Pacheco, J. G.; Nouws, H. P. A.; Albergaria, J. T.; Delerue-Matos, C.** *Sci. Total Environ.*, **2015**, **533**, 76–81.
20 **Kammler, H. K.; Mädler, L.; Pratsinis, S. E.** *Chem. Eng. Technol.*, **2001**, **24**, 583–596.
21 **Ndolomingo, M. J.; Meijboom, R.** *Appl. Surf. Sci.*, **2016**, **390**, 224–235.
22 **Önal, E. S.; Yatkın, T.; Aslanov, T.; Ergüt, M.; Özer, A.** *Int. J. Chem. Eng.*, **2019**, **2019**, 2716423.
23 **Li, N.; Zhao, P.; Astruc, D.** *Chem. Eur. J.*, **2014**, **53**, 1756–1789.
24 **Lara, P.; Philippot, K.** *Catal. Sci. Technol.*, **2014**, **4**, 2445–2465.
25 **Kumar, S. S.; Venkateswarlu, P.; Rao, V. R.; Rao, G. N.** *Int. Nano Lett.*, **2013**, **3**, 1–6.
26 **Khan, A.; Rashid, R.; Murtaza, G.; Zahra, A.** *Trop. J. Pharm. Res.*, **2014**, **13**, 1169–1177.
27 **Danhier, F.; Ansorena, E.; Silva, J. M.; Coco, R.; Le Breton, A.; Préat, V.** *J. Control. Release*, **2012**, **161**, 505–522.
28 **Mura, S.; Couvreur, P.; Nicolas, J.** *Nat. Mater.*, **2013**, **12**, 991–1003.
29 **Immordino, M. L.; Dosio, F.; Cattel, L.** *Int. J. Nanomedicine*, **2006**, **1**, 297–315.
30 **Shah, P.; Gavrin, A.** *J. Magn. Magn. Mater.*, **2006**, **301**, 118–123.
31 **Chen, Y.; Dalwadi, G.; Benson, H.** *Curr. Drug Deliv.*, **2004**, **1**, 361–376.
32 **Sun, L.; Singh, A. K.; Vig, K.; Pillai, S. R.; Singh, S. R.** *J. Biomed. Nanotechnol.*, **2008**, **4**, 149–158.
33 **Hasan, S. A.** *Res. J. Recent Sci.*, **2015**, **4**, 1–3.
34 **Kammler, H. K.; Mädler, L.; Pratsinis, S. E.** *Chem. Eng. Technol.*, **2001**, **24**, 583–596.
35 **Palei, N. N.; Mohanta, B. C.; Sabapathi, M. L.; Das, M. K.** *Org. Mater. Smart Nanocarriers Drug Deliv.*, **2018**, **1**, 415–470.